A combined integro-modal approach for predicting acoustic properties of irregular-shaped cavities

J. Missaoui and L. Cheng
Department of Mechanical Engineering, Laval University, Québec, Québec G1K 7P4, Canada

An integro-modal approach is presented in this paper for computing the acoustic properties of irregular-shaped cavities. The method consists of discretizing the whole cavity into a series of subcavities, whose acoustic pressure is decomposed either over a modal basis of regular subcavities or over that of the bounding cavities in the case of irregular-shaped boundaries. An integral formulation is then established to ensure continuity of both pressure and velocity between adjacent subcavities using a membrane with zero mass and stiffness. To some extent, the method provides a combined approach retaining the advantages of both the acoustoelastic method (AEM) and the Green's function method (GFM). Numerical and experimental results are presented demonstrating the efficiency and accuracy of the suggested technique. Comparisons with other existing methods are also made. It is shown that good accuracy on the computation of cavity modes can be obtained using a very limited number of subcavities. © *1997 Acoustical Society of America.* [S0001-4966(97)04806-6]

INTRODUCTION

Interior noise associated with surrounding vibrating structures has been the subject of many studies. One typical example is the cabin noise of aircraft and vehicles with vibrating walls which frequently create noise levels exceeding the human comfort limits. In such applications, irregular-shaped cavities are often involved, whose modal characteristics are fundamental to a better understanding of the sound radiation mechanism and any noise reduction action that needs to be taken.

Analytical expressions are available to calculate natural frequencies and mode shapes of regular cavities. Unfortunately, only a few simple geometries such as rectangular and cylindrical cavities allowing the separation of the variables can be simply treated by classical methods. As far as other cavities with an arbitrary shape are concerned, the literature shows that the available methods are quite limited. The most popular alternatives are numerical methods[1–4] such as finite element method (FEM). This method has been widely and successfully used in the past to analyze irregular cavities. The main disadvantage is the large number of degrees required and the related computation time. Other methods involving a more physical basis rather than numerical ones have been also developed. In Ref. 5 an acoustoelastic model (AEM) was used to determine acoustic natural frequencies of multiply connected regular cavities. The method was then extended in Ref. 6 to compute the acoustic modal properties of irregular-shaped cavity. The procedure is based on an approximation of the cavity geometry by a set of rectangular subcavities. Adjacent subcavities are jointed together by means of vibrating membranes. Although only rectangular subcavities were used in this work, it is natural to suppose that other regular subcavities can also be used if they admit analytical solutions. However, the disadvantage of this approach lies in the fact that the number of subcavities required is highly dependent on the irregularity of the cavity shape.

Approximating the cavity geometry by a series of regular shapes introduces inevitable errors in the computation. Another approach, based on the Green's function method (GFM) was described in Ref. 7. A practical application of this method was reported by Succi[8] who calculated the acoustic response of an automobile cabin by imposing the vibration of panels on the cavity boundary. The method is very helpful since there is no need to calculate the acoustic modes as far as the structural-acoustic response is concerned. The method is limited however to a cavity only slightly distorted from a regular one.

In the present paper an alternative approach is presented for computing the acoustic properties of cavities of arbitrary shape. This method is based on an integro-modal formulation combining the advantages of the two methods mentioned above (AEM and GFM). It permits the use of mixed subcavities, of either regular or irregular shape, leading to a minimal discretization. The modal characteristics of regular subcavities are obtained analytically while the irregular subcavities are treated using a modal expansion over the mode shapes of their regular bounding cavities. An integral formulation is then established to ensure both the continuity of the pressure and velocity between adjacent subcavities using a membrane with zero mass and stiffness. In regard to AEM, both regular and irregular subcavities can be used in this approach. In doing this the approximation is related to the solution, rather than the cavity shape. One would expect that the solution converges more rapidly using fewer subcavities. Compared to GFM, the fact that the bounding cavities can be taken for each subcavities makes it possible to choose envelopes even if the cavity is strongly irregular. As a result, envelopes closer to the subcavity geometries can be used to enhance the prediction accuracy.

The mathematical formulation is described in Sec. I for an irregular-shaped cavity. Numerical results are then presented in Sec. II. Several configurations are then used to

study the convergence of the method and to validate the theory. In each case, resonant frequencies of the cavity computed using the present approach are compared with results reported in the literature. An experimental validation is also reported in Sec. III.

I. FORMULATION

The mathematical formulation consists in treating an irregular-shaped cavity as a combination of connected subcavities separated by elastic panels. In each subcavity, the interior sound pressure p can be calculated by transforming the Helmholtz equation into an integral form via the second Green's theorem.

$$\int_V G(\nabla^2 p + \lambda^2 p) dv = \int_V p(\nabla^2 G + \lambda^2 G) dv$$
$$+ \int_{S_b} \left(G \frac{\partial p}{\partial \mathbf{n}} - p \frac{\partial G}{\partial \mathbf{n}} \right) ds, \qquad (1)$$

where λ is the wave number; $\mathbf{n}$ the outward normal vector of the boundary surface S_b of the enclosure with volume V; G the Green's function corresponding to a transfer function obtained between an observation point (r) and the source (r_0). The construction of the function G for a Neumann boundary is based on the inhomogeneous Helmholtz equation with an infinite surface impedance written as follows:

$$\nabla^2 G(r,r_0) + \lambda^2 G(r,r_0) = -\delta(r-r_0),$$
$$\frac{\partial G(r,r_0)}{\partial \mathbf{n}} = 0, \qquad (2)$$

in which $\delta(r-r_0)$ is the Dirac delta function. The analytical expression for the function G satisfying Eq. (2) and using normal modal expansion can be written as follows:

$$G(r,r_0) = \sum_n \frac{c^2 \varphi_n(r) \varphi_n(r_0)}{(\omega_n^2 - \omega^2) V \wedge_n}, \qquad (3)$$

where c is the speed of the sound in the internal medium, ω_n is the angular resonance frequency of the cavity, φ_n the corresponding mode shape and $\wedge_n = (1/V) \int_v \varphi_n^2(r) dv$ the generalized acoustic mass.

An irregular-shaped cavity may be composed of both regular and irregular subcavities, each of which being treated differently hereafter. For illustration purposes, the formulation is first developed for the cavity shown in Fig. 1(a). The whole process will then be generalized. As illustrated in Fig. 1, the cavity investigated can be divided into a regular [Fig. 1(b)] and an irregular [Fig. 1(c)] subcavity. The junction between the two subcavities is replaced by a vibrating panel. These two subcavities are first treated separately and then coupled together by harmonizing the motion of the panel.

A. Regular subcavity

In the case of a regular-shaped cavity, analytical expressions are available for the mode shapes and the natural frequencies. Typical examples are rectangular, cylindrical, or semi-cylindrical enclosures. Based on a fluid formulation,
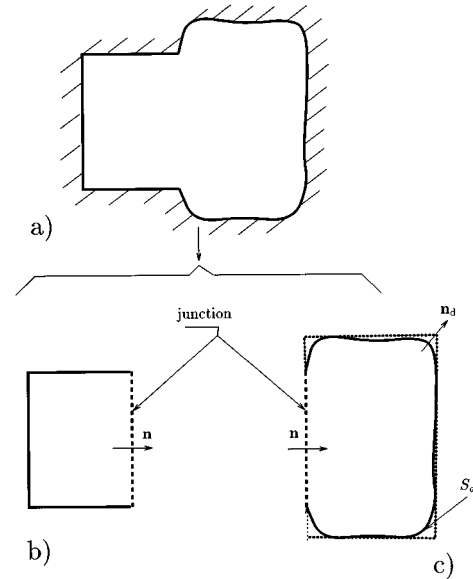
FIG. 1. Discretization procedure used in the present approach. (a) Real cavity; (b) regular subcavity; panel: -----; (c) irregular subcavity; panel: -----; bounding cavity: ....

the internal pressure is decomposed using an orthogonal expansion in terms of the hard-walled cavity modes:

$$p = \rho_f c^2 \sum_n \frac{a_n(t)}{\wedge_n} \varphi_n(r), \qquad (4)$$

where ρ_f is the fluid density, n the modal indices of the cavity, and $a_n(t)$ the modal pressure amplitudes to be determined. The transverse displacement of the vibrating wall w is also expanded in terms of *in vacuo* normal mode shapes ψ_m:

$$w = \sum_m q_m(t) \psi_m, \qquad (5)$$

where m contains the structural modal indices; $q_m(t)$ are the structural modal coordinates. Assuming that no absorbent boundary conditions are present and that the interior noise is due to arbitrary vibrating surfaces with the remaining part being acoustically hard wall, the substitution of Eqs. (3), (4), and (5) in Eq. (1) leads to a linear modal acoustic equation:

$$\ddot{a}_n + \omega_n^2 a_n = -\frac{A_f}{V} \sum_m \ddot{q}_m L_{nm}, \qquad (6)$$

where A_f is the area of the vibrating surface and

$$L_{nm} = \frac{1}{A_f} \int_s \varphi_n(r) \psi_m(r) ds, \qquad (7)$$

with L_{nm} being the modal coupling coefficient between the mth structure mode and the nth cavity mode. This term characterizes the coupling in space between the two modes.

B. Irregular subcavity

An irregular-shaped subcavity may be considered as a deviation from a regular shape, as shown in Fig. 1(c). In this section the procedure consists of enclosing the irregular cavity by a regular one, called the envelope or bounding cavity,

for which modal information is available. Since the natural modes of the irregular-shaped cavity are not known analytically, the modes of the bounding cavity ϕ are then used to perform the pressure decomposition in a similar way to that illustrated in Eq. (3), by replacing φ by ϕ. Similarly, the Green's function can also be obtained. Except for the flexible part, all the remaining boundary are supposed to be acoustically hard. Equation (1) hence becomes

$$
\sum_n \frac{a_n(t)}{\wedge_n} \phi_n(r) = -\frac{c^2}{V} \sum_{n'} \sum_n \frac{\phi_n(r)}{(\omega_n^2 - \omega^2)\wedge_n} \frac{a_{n'}(t)}{\wedge_{n'}}
$$
$$
\times \int_{S_d} \phi_{n'}(r_0) \frac{\partial \phi_n(r_0)}{\partial \mathbf{n}_d} ds
$$
$$
- \frac{A_f}{V} \sum_m \sum_n \frac{\ddot{q}_m \phi_n(r) L_{nm}}{\wedge_n (\omega_n^2 - \omega^2)}, \tag{8}
$$

where V, ω_n, and $\wedge_n$ belong to the bounding cavity; S_d is the surface of the irregular subcavity with a unit normal vector $\mathbf{n}_d$. L_{nm} is again the coupling coefficient defined in Eq. (7), after replacing φ by ϕ. Using the orthogonality principle of the eigenfunction of the bounding cavity, the following modal equation is obtained:

$$
\ddot{a}_n + \omega_n^2 a_n + \frac{c^2}{V} \sum_{n'} \frac{a_{n'}}{\wedge_{n'}} \int_{S_d} \phi_{n'} \frac{\partial \phi_n}{\partial \mathbf{n}_d} ds
$$
$$
= -\frac{A_f}{V} \sum_m \ddot{q}_m L_{nm}. \tag{9}
$$

In Eq. (9), the integration is performed over the surface of the irregular cavity, either analytically or numerically, depending on the complexity of the shape. One can see that any irregularity of the boundary shape has the effect of coupling the acoustic modes of its envelope. One property of the integral term can be evaluated from the Helmholtz equation by the following simple expression:

$$
(\omega_{n'}^2 - \omega_n^2) \int_{V_d} \phi_n \phi_{n'} dv = c^2 \left(\int_{S_d} \phi_{n'} \frac{\partial \phi_n}{\partial \mathbf{n}_d} ds \right.
$$
$$
\left. - \int_{S_d} \phi_n \frac{\partial \phi_{n'}}{\partial \mathbf{n}_d} ds \right). \tag{10}
$$

In the special case where both cavities coincide, the hard wall condition gives:

$$
\int_S \phi_{n'} \frac{\partial \phi_n}{\partial \mathbf{n}} ds = \int_S \phi_n \frac{\partial \phi_{n'}}{\partial \mathbf{n}} ds = 0. \tag{11}
$$

Consequently, Eq. (10) shows the orthogonality relations between the acoustic modes

$$
\int_V \phi_n \phi_{n'} dv = 0; \quad n \neq n'. \tag{12}
$$

It should be observed that Eq. (9) is a more general form than Eq. (6). Hence, in the following development Eq. (9) is retained as a characteristic equation of the subcavities.

C. Coupling between the two subcavities

The cavity illustrated in Fig. 1(a) has been discretized to a regular and an irregular subcavity, connected by elastic panel, as shown in Fig. 1(b) and (c). The acoustic pressure difference across the interconnected region is governed by the vibrations of the elastic panel. The pressure jump $\bar{p}$ and the normal gradient pressure jump on both sides ($+$ and $-$) of the panel can be expressed respectively as:

$$
\bar{p} = \rho_f c^2 \left(\sum_n \frac{a_n}{\wedge_n} \phi_n \right)^+ - \rho_f c^2 \left(\sum_n \frac{a_n}{\wedge_n} \phi_n \right)^-,
$$
$$
\frac{\partial \bar{p}}{\partial \mathbf{n}} = \rho_f c^2 \left(\sum_n \frac{a_n}{\wedge_n} \frac{\partial \phi_n}{\partial \mathbf{n}^+} \right)^+ - \rho_f c^2 \left(\sum_n \frac{a_n}{\wedge_n} \frac{\partial \phi_n}{\partial \mathbf{n}^-} \right)^-. \tag{13}
$$

These two quantities depend on the structural properties. In fact, the panel is exposed to an acoustic pressure loading on both sides. Assuming a harmonic behavior for the whole system [$a_n(t) = P_n \sin(\omega t)$ for sound pressure and $q_m(t) = U_m \sin(\omega t)$ for the panel], the governing equation of motion of a thin isotropic panel may be used:

$$
D_s \nabla^4 w + \rho_s h_s \frac{\partial^2 w}{\partial t^2} = p^+ - p^-, \tag{14}
$$

where D_s is the bending stiffness and ρ_s and h_s are, respectively, the mass density and the thickness of the panel, and ∇^4 is the biharmonic operator. Substituting Eq. (5) into Eq. (14) and using the orthogonality property of the structural modes, Eq. (14) is then transformed into a modal structural equation given by:

$$
M_m(\omega_m^2 - \omega^2) q_m = \int_{A_f} p^+ \psi_m \, ds - \int_{A_f} p^- \psi_m \, ds, \tag{15}
$$

where M_m is the structural generalized mass and ω_m the angular structural resonant frequency. In the real physical system, which is a combination of a series of subcavities, such a panel does not really exist. The purpose of the above formulation, using a panel, is just an artificial means to simulate the continuity between adjacent subcavities. Therefore, one can imagine a massless and stiffness-free membrane existing to separate the subcavities. As a special case of Eq. (15) by neglecting the generalized mass, the equation is reduced to

$$
\int_{A_f} p^+ \psi_m \, ds - \int_{A_f} p^- \psi_m ds = 0. \tag{16}
$$

For each subsystem (subcavity+membrane), the above equation will be used, together with the modal acoustic equation (9), to handle a more general case composed of a number of subsystems.

D. Generalization of the formulation

In order to generalize the procedure, the four subcavity system shown in Fig. 2(a) and (b) was first investigated. From the topological description illustrated in Fig. 2(b), Eq. (9) is applied to each subcavity k ($k=1,2,3,4$) and Eq. (16) for each membrane. This procedure results in the following
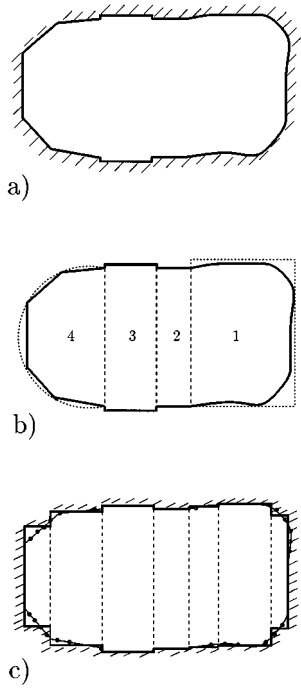
FIG. 2. Comparison between discretization procedures. (a) Real cavity; (b) discretization procedure used in the present approach; real cavity: —; bounding cavity: ....; panel: ------; (c) discretization procedure used in the acoustoelastic approach; real cavity: •-•-•-•; subcavities: —; panel: ------.

equations, expressed in matrix form, describing the coupling between the vectors P and U comprised respectively of the acoustic and structural modal amplitudes:

$$[A_k]\{P^k\} - [B_{k,k}]\{U^k\} = 0, \quad k=1,$$

$$[A_k]\{P^k\} + [B_{k,k-1}]\{U^{k-1}\} - [B_{k,k}]\{U^k\} = 0, \quad k=2,3, \quad (17)$$

$$[A_k]\{P^k\} + [B_{k,k-1}]\{U^{k-1}\} = 0, \quad k=4,$$

where the components of matrices $[A]$ and $[B]$ are

$$[A_k]_{ij} = (\omega_{ik}^2 - \omega^2)\delta_{ij} + \frac{c^2}{\wedge_j V} \int_s \phi_j^k \frac{\partial \phi_i^k}{\partial \mathbf{n}_d^k},$$

$$[B_{k,k}]_{ij} = \omega^2 \frac{A_f^k}{V^k} [L_{k,k}]_{ij},$$

$$[B_{k,k-1}]_{ij} = \omega^2 \frac{A_f^{k-1}}{V^k} [L_{k,k-1}]_{ij},$$

where δ_{ij} is the Kronecker parameter and $[L]$ is the coupling matrix. Note that the first and the third equations hold for the two subcavities at the two ends with one separating membrane. The second equation is for the two intermediate subcavities which have two separating membranes at each end. On the other hand, the application of the modal structural equation Eq. (16) for each membrane leads to a set of equations summarized in the following matrix form:

$$[C_{k,k}]\{P^k\} - [C_{k+1,k}]\{P^{k+1}\} = 0, \quad k=1,2,3, \quad (18)$$

where the components of the matrix $[C]$ can be calculated from:

$$[C_{k,k}]_{ij} = \frac{1}{\wedge_j^k} [L_{k,k}]_{ji},$$

$$[C_{k+,1k}]_{ij} = \frac{1}{\wedge_j^{k+1}} [L_{k+1,k}]_{ji}.$$

Equation (18) describing the pressure continuity at the interface between adjacent portions can also be formulated in terms of the unknown vectors U containing the structural modal amplitudes. In fact, substituting Eqs. (17) into Eq. (18) gives

$$\sum_{j=0}^{1} [-C_{k+j,k} A_{k+j}^{-1} B_{k+j,k}]\{U^k\} + [C_{k+1,k} A_{k+1}^{-1} B_{k+1,k+1}]$$

$$\times \{U^{k+1}\} = 0, \quad k=1,$$

$$[C_{k,k} A_k^{-1} B_{k,k-1}]\{U^{k-1}\} + \sum_{j=0}^{1} [-C_{k+j,k} A_{k+j}^{-1} B_{k+j,k}]$$

$$\times \{U^k\} + [C_{k+1,k} A_{k+1}^{-1} B_{k+1,k+1}]\{U^{k+1}\} = 0, \quad k=2,$$

$$\tag{19}$$

$$[C_{k,k} A_k^{-1} B_{k,k-1}]\{U^{k-1}\} + \sum_{j=0}^{1} [-C_{k+j,k} A_{k+j}^{-1} B_{k+j,k}]$$

$$\times \{U^k\} = 0, \quad k=3.$$

In the more general case in which N subcavities are involved, this discretization procedure may be generalized. In fact, the governing equations for $k=1$ and $k=4$ can be directly applied to the first and the last subcavity of an arbitrary system, while the equations for $k=2,3$ hold for all intermediate subcavities. Furthermore, Eq. (18) applies to all membranes. The complete procedure yields the following general equation.

$$[Q]\{U\} = 0; \quad \{U\} = \{U^1, U^2, ..., U^{N-1}\}^T. \tag{20}$$

Submatrices constituting the above system can calculated as follows:

$$[Q_{i,j}] = -[C_{i,i} A_i^{-1} B_{i,i}] - [C_{i+1,i} A_{i+1}^{-1} B_{i+1,i}], \quad i=j,$$

$$[Q_{i,j}] = [C_{ji} A_j^{-1} B_{j,j}], \quad j=i+1,$$

$$[Q_{i,j}] = [C_{ii} A_i^{-1} B_{i,j}], \quad i=j+1, \tag{21}$$

$$[Q_{i,j}] = 0, \quad |i-j| \geq 2.$$

It can be seen from these equations that the global $[Q]$ matrix is a banded one. This property is very helpful for reducing the final size of the matrix to be treated. In fact, using a partitioning technique of linear algebra for the banded matrix, any linear system can be reduced to a simple form involving only one set of modal coordinates. For example, if one chooses the coordinate set related to the first membrane $\{U^1\}$, successive substitutions yields

$$\{U^1\} = [H_1]\{U^1\}, \quad \{U^2\} = [H_2]\{U^1\},$$

$$\{U^k\} = [H_k]\{U^1\}; \quad 3 \leq k \leq N-1, \tag{22}$$

where

$$[H_1]=[I], \quad [H_2]=-[Q_{1,2}^{-1}Q_{1,1}],$$
$$[H_k]=-[Q_{k-1,k}^{-1}][Q_{k-1,k-2}+Q_{k-1,k-1}H_{k-1}], \tag{23}$$
$$3 \leqslant k \leqslant N-1.$$

This whole procedure transforms the system expressed by Eq. (21) into a much more compact form using only the coordinates related to the first membrane:

$$\left[C_{k,k}A_k^{-1}B_{k,k-1}H_{k-1} - \sum_{j=0}^{1} C_{k+j,k}A_{k+j}^{-1}B_{k+j,k}H_k \right]\{U^1\}$$
$$=0, \quad k=N-1. \tag{24}$$

Equation (24) should be solved to calculate the resonant frequencies. Note that Eq. (24) is a nonstandard eigenvalue problem so that numerical methods such as the bisection method should be used by making a distinction between poles and true solutions. The modal structural amplitude vector U^1 can then be calculated. A back substitution into Eq. (22) then gives all the other vectors U_k. Modal sound-pressure vectors P for each subcavity can then be computed from Eq. (17). For each resonant acoustic frequency ω_a, the modal shape of the cavity can also be evaluated using Eq. (4).

At this stage it is of interest to highlight the difference between the present formulation and the acoustoelastic method (AEM) concerning the discretization procedure. One particular aspect of the AEM, as illustrated in Fig. 2(c), is that the discretization introduces an approximation in the geometry of the irregular cavity, since the cavity, in practice, is replaced by a a series of regular-shaped subcavities whose boundaries deviate more or less from the real cavity boundary. In the proposed integro-modal method (IMM), no such geometry approximation is necessary. Although the natural modes of the bounding cavity are used, it is the subcavities with real boundaries that are treated as shown in Fig. 2(b). From this point of view, the IMM is expected to be more accurate than the AEM while using fewer subcavities. On the other hand, the partitioning technique on the band matrix adopted here considerably reduces the size of the final matrix. Consequently, storage requirements are less demanding, permitting a substantial reduction in computation time.

II. NUMERICAL RESULTS

A. Remarks on numerical solution

The solution of Eq. (24) depends on the modal properties of the uncoupled component of each subsystem and the discretization of the whole enclosure. The truncation to a finite order of the decomposition series for both acoustic pressure and the membrane vibration and the number of subcavities used should be the two main factors affecting the accuracy of the method. Therefore, a convergence analysis of the method concerning these parameters is required. In order to ensure good convergence, three indices should be determined: the number of subcavities and the number of terms used in each of the acoustic and membrane series in Eqs. (4) and (5). For a given cavity, one can start with a small num-
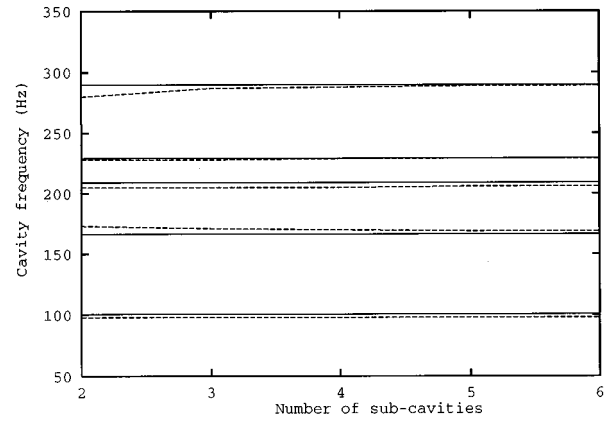
FIG. 3. Convergence study as a function of subcavity number for a semicircular enclosure with unit radius. Exact: —; present approach: ----- with $n_a=10$; $m_s=10$.

ber of subcavities to get a rough idea about the frequency range of the modes of interest. The number of decomposition terms for each series can then be increased until no significant change is observed. Another cycle follows by increasing the number of subcavities and repeating the procedure for the decomposition series. This procedure should give the appropriate number of indices required to ensure a convergent stable solution. For a two-dimensional problem, two indices corresponding to the two orthogonal directions are involved for each acoustic mode. The maximum values of these indices are denoted by n_x and n_y. In all calculations reported hereafter, these two indices are always set equal; $n_x=n_y=n_a$. As far as the membrane is concerned, only one index is necessary, with m_s standing for the maximum number of terms used in the decomposition series.

In order to demonstrate the convergence properties of the method, a semi-circular cavity with a unit radius was investigated. In the calculations, rectangular bounding enclosures were used for each subcavity. The fluid speed inside the cavity was taken to be 343 m/s. The calculated natural frequencies are compared with the analytical solution given by:

$$\omega_{psq}=c\sqrt{\gamma_{ps}^2+(q\pi/l)^2}, \tag{25}$$

where psq are the modal indices of the semi-cylindrical cavity of length l and radius a, γ_{ps} is the value of the sth root of the Bessel function of the first kind and order p: $J_p'(\gamma_{ps}a)=0$. Since a two-dimensional problem is considered here, one has $q=0$.

The first example concerns convergence with respect to the number of subcavities, keeping the number of decomposition terms constant at an appropriate value (i.e., $n_a=10$, meaning that 100 modes are used for each subcavity and 10 terms for each membrane). The convergence curves of the first five acoustic modes using the present method are compared with the exact solution in Fig. 3. It can be seen from Fig. 3 that the convergence rate depends on particular mode and that the computed solutions agree closely with the exact values. It is also worth noting that the solution seems to be
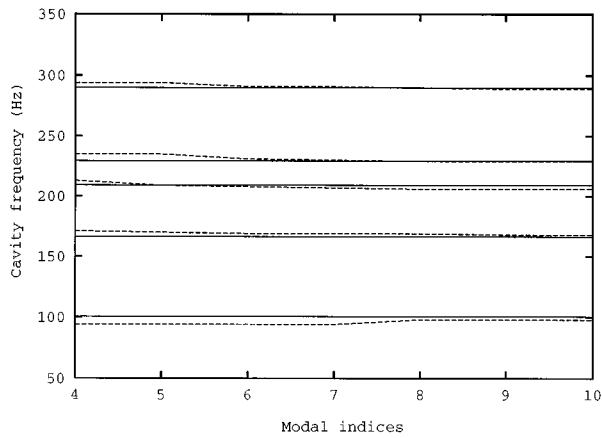
FIG. 4. Convergence study as a function of the modal indices of each subsystem. Exact: —; present approach: -----. The semi-circular enclosure is discretized by $N=5$ subcavities.

quite stable with a small number of subcavities, and relatively insensitive to any further increase in the number of subcavities.

Using five subcavities ($N=5$), the same investigation was carried out varying the number of terms in the different series. For the sake of convenience, the same values were taken for all the indices involved ($n_a=m_s$) and were increased accordingly. Comparisons with the analytical solution are presented in Fig. 4. Again, the calculated frequencies seem to converge quickly and closely to the exact solution with the increase in the number of decomposition terms.

A few remarks are necessary regarding the numerical technique for the calculation of the natural frequencies. As mentioned before, the bisection method is used in the present work by making a distinction between poles and true solutions to find the roots of the characteristic equation of the nonstandard eigenvalue problem. This procedure is illustrated in Fig. 5 based on the cavity treated previously. In this
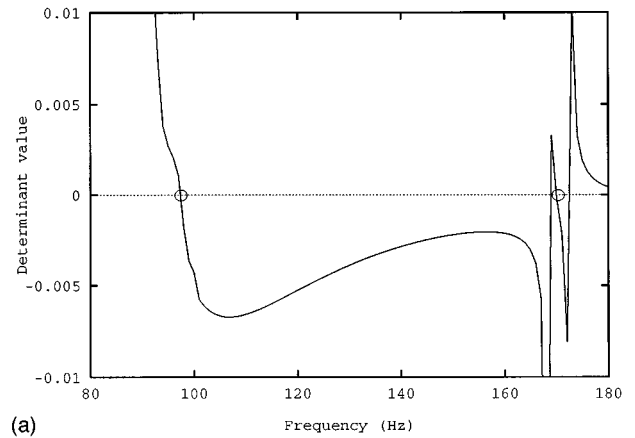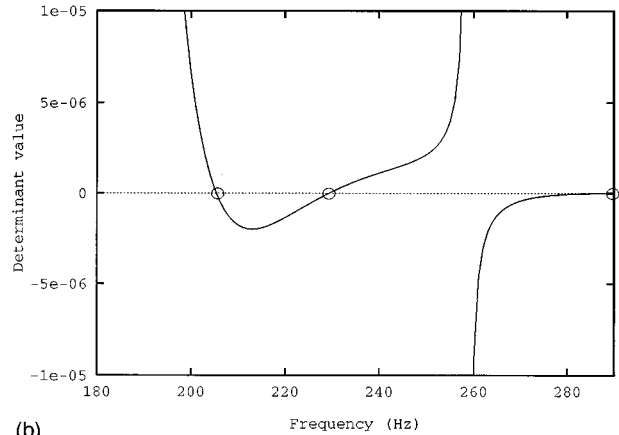
FIG. 5. Graphical representation of computed solutions of a semi-circular enclosure with $N=5$; $n_a=10$; $m_s=10$. (a) Frequency range 80–180 Hz; (b) frequency range 180–290 Hz.

figure, the determinant of Eq. (24) is plotted in Fig. 5(a) and 5(b) over a frequency band ranging from 80 to 290 Hz, comprising the five first modes. As can be seen, the presence of poles changes locally the property of the characteristic equa-

TABLE I. Resonant frequencies of a semi-circular enclosure with unit radius: A comparison between the present approach ($N=5$; $n_a=m_s=10$), the acoustoelastic method ($N=15$; $n_a=m_s=10$) and the exact solution.

Mode order	Exact solution f_n (Hz)	Present approach		Acoustoelastic method	
		f_n (Hz)	Error (%)	f_n (Hz)	Error (%)
1	100.4459	98.0	−2.43	100.0	−0.44
2	166.4999	168.0	0.90	165.0	−0.90
3	209.0803	206.0	−1.47	210.0	0.44
4	229.2786	229.0	−0.12	229.0	−0.12
5	289.8737	289.0	−0.30	287.0	−0.99
6	290.9655	295.0	1.38	293.0	0.70
7	349.9228	354.0	1.16	346.0	−1.12
8	365.7540	369.0	0.88	367.0	0.34
9	382.6769	383.0	0.08	386.0	0.86
10	409.4261	412.0	0.63	404.0	−1.32
11	437.2671	437.0	−0.06	440.0	0.62
12	465.6539	463.0	−0.57	457.0	−1.85
13	467.8375	475.0	1.53	468.0	0.03
14	506.5966	510.0	0.67	508.0	0.27
15	526.2490	532.0	1.09	519.0	−1.37
16	543.7178	544.0	0.05	546.0	0.42
17	555.1818	554.0	−0.21	559.0	0.68
18	573.7424	567.0	−1.17	565.0	−1.52
19	584.6605	583.0	−0.28	576.0	−1.48
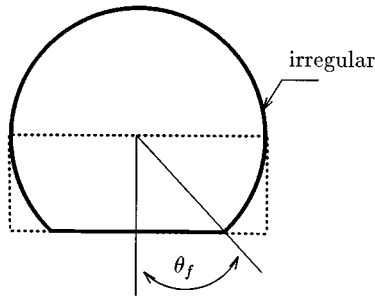
FIG. 6. A two-dimensional simplified aircraft cabin: —; bounding cavity: ....

FIG. 7. Acoustic frequencies of a two-dimensional simplified aircraft cabin with unit radius and a floor location of $\theta_f = 56.6°$. Frequencies calculated using the present approach with $N=2$: $- \cdot - \cdot - \cdot$; the acoustoelastic method with $N=5$: -----; the finite difference method in Ref. 12: —.

tion. These poles correspond to subcavity frequencies which make the matrix $[A_k]$ singular so that they are not the true resonant frequencies of the whole cavity. In our case, for example, the first solution is a true root, while the second one is a pole. For the whole frequency range under consideration, all five roots are marked by a circle in the various plots [Fig. 5(a) and (b)].

B. Validation and comparison with other methods

Validation tests were also performed using the regular cavity cited above and another geometry simulating a simplified two-dimensional aircraft cabin, including comparisons with other available methods. All the simulations used $n_a = m_s = 10$ with a variable number of subcavities.

1. Semi-circular cavity

Again, the semi-circular cavity used before was investigated. The computed results of cavity frequencies for a frequency range of 90–600 Hz are reported in Table I, together with a comparison between the present method (IMM), the acoustoelastic method (AEM), and the analytical solution. It can be observed that both methods agree well with the analytical solutions. The mean percentage error (calculated with absolute values) over the whole frequency range is about 0.8% for both methods. However, only 5 subcavities were used in the present method while 15 subcavities were used in AEM. Also, the present approach needs 30% of the discretization size of the AEM. From this point of view, the proposed approach seems to be more efficient than the AEM to achieve comparable accuracy.

2. Two-dimensional simplified aircraft cabin

Another computational example was performed on a simplified aircraft cabin with an irregular shape. This configuration is of great interest in recent research on aircraft cabin noise.[9–11] The addition of the floor to the cylindrical model leads to a more realistic configuration compared with the single cylindrical model reported frequently in the literature, but results in a cavity cannot be treated by analytical methods. The cavity geometry is illustrated in Fig. 6. The proposed method is applied to this configuration which is discretized into two subcavities: an upper semi-circular cavity coupled to a lower irregular cavity with a rectangular envelope. It is equally possible to use a semi-circular enve-

lope for the lower subcavity. The acoustoelastic coupling between the semi-circular cavity and the membrane is evaluated by a numerical integration over the vibrating surface. The modal coupling coefficient is given by
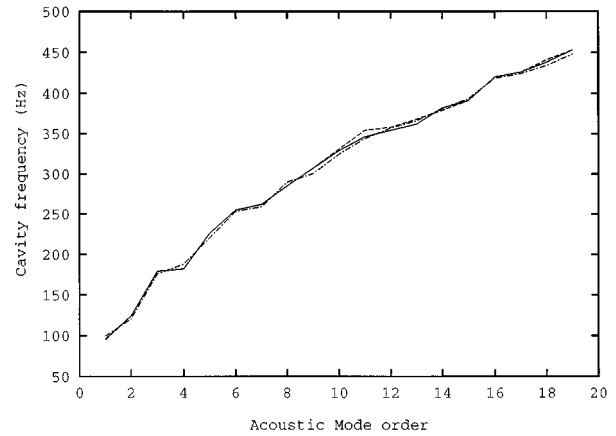
$$
L_{psm} = \frac{1}{A_f} \int_0^a J_p(\gamma_{ps} r) \left[\sin\left(\frac{m\pi(r+a)}{2a} \right) \right.
$$
$$
\left. + (-)^p \sin\left(\frac{m\pi(a-r)}{2a} \right) \right] dr, \qquad (26)
$$

where (p,s) are the acoustic modal indices and a is the radius of the semi-circle. With an angle of $\theta_f = 56.6°$ defining the position of the floor, different results regarding the natural frequencies are compared in Fig. 7. The results used were calculated respectively by IMM, AEM, and also taken from Ref. 12 based on the finite difference approach. The IMM used two subcavities while the AEM used five. The agreement between the three methods is reasonably good. Once again, comparable accuracy was obtained using IMM, with less subcavities than the AEM.

One of the appealing features of the IMM is its flexibility in choosing different strategies to handle different configurations. As an example, consider the cabin configuration

TABLE II. Resonant frequencies of a simplified cabin with a floor location of $\theta_f = 49°$ and a unit radius: A comparison between the present approach ($N=1$; $n_a = 10$) and Ref. 13.

Mode order	Reference 13 f_n (Hz)	Present approach	
		f_n (Hz)	Error (%)
1	96.416	95.0	−1.47
2	113.002	117.0	3.53
3	166.997	173.0	3.60
4	178.748	179.0	0.14
5	212.718	217.0	2.01
6	238.019	244.0	2.51
7	243.915	252.0	3.31
8	280.915	283.0	0.74
9	283.663	288.0	1.53
10	305.542	295.0	−3.45
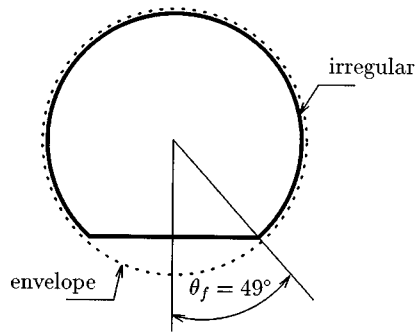
FIG. 8. Discretization of a two-dimensional simplified aircraft cabin of unit radius using one subcavity. The floor location is at $\theta_f = 49°$.

TABLE III. Resonant frequencies of a simplified cabin with a floor location of $\theta_f = 49°$ and a 0.254 m radius. A comparison between the present approach ($N=2$; $n_a = m_s = 10$) and experimental results.

Mode order	Experimental results f_n (Hz)	Present approach	
		f_n (Hz)	Error (%)
1	380.0	375.0	−1.31
2	460.0	463.0	0.65
3	678.0	684.0	0.88
4	720.0	710.0	−1.39
5	848.0	856.0	0.94
6	968.0	963.0	−0.51

with $\theta_f = 49°$ and unit radius, as in Fig. 8. The fact that the floor position is lower than the previous one makes the cavity closer to a completely circular one. In this case, the enclosure can be treated as one single cavity with a complete circular envelope. In this case, only Eq. (9) is needed with the left hand side term equal to zero, since no membrane is present in the system. A comparison with Ref. 13 is given in Table II. It can be observed that, although the agreement is acceptable, the error is greater than that obtained previously. This can certainly be attributed to the deviation in the boundary shape, since even with the low floor position it is still quite different from the envelope. Accuracy can certainly be enhanced by using more subcavities at the price of increasing the calculation effort.

III. EXPERIMENTAL VALIDATION

Experimental tests were performed to assess the proposed method on a cavity simulating an aircraft cabin. The experimental setup and instrumentation used are illustrated in Fig. 9. The cavity was formed by a steel cylinder with a floor. The interior space of concern was the volume above the floor. The ends of the cavity were closed with thick steel end caps. The test cylinder had an internal diameter of 0.504 m and was 1.1684 m long. The floor was made of the same material as the cylinder and was located at an angle θ_f of 49°. Two $\frac{1}{2}$-in. microphones were placed inside the cavity supported by a thin tube along the cylinder centerline. The tube could be rotated and moved along the centerline to pick

out any desired measurement point. Acoustic excitation was produced by a loudspeaker with a cone connector fixed to the right end cap through a hole. The characteristics of the cone connector was chosen in such a way that neither its acoustic nor its structural resonances lie in the frequency range of interest. The measured sound pressure was treated by a multi-channel BK 3550 FFT analyzer. Care was taken to avoid any strong coupling between the cavity and the boundary formed by structure. It was observed that stiffening the structure did not noticeably change the measured resonant frequencies. Although more than a dozen resonant modes were clearly identified, only the two-dimensional modes, corresponding to modes in the cross section are compared with our calculations in Table III. The values of these two-dimensional modes can be used to derive the other three-dimensional modes involved, since simple formulas are available for the longitudinal direction. It can be seen that the theoretical results and the experimental measurements agree well with a maximal error of 1.3%.

IV. CONCLUSION

A new approach has been proposed for the computation of acoustic modes of irregular-shaped cavities. The method approximates the solution via an integro-modal formulation using multi-connected subcavities. The formulation is general and flexible enough to handle different cavity configurations. From this point of view, the Green's function method can be considered as a special case of the present technique using one single bounding cavity. With respect to the acoustoelastic method, the proposed formulation permits the use of irregular-shaped subcavities, thus making the approach more powerful. Numerical results on two-dimensional cavities have been presented to demonstrate the efficiency and the accuracy of the approach. Preliminary comparisons with the acoustoelastic method shows that the proposed technique gives comparable results using fewer subcavities.

Future work is required to extend this approach to the prediction of interior noise inside irregular-shaped cavity coupled with vibrating structures.

FIG. 9. Experimental setup: (1): cylinder; (2): floor; (3): end caps; (4): $\frac{1}{4}$-in. microphones; (5): tube; (6): loudspeaker; (7): connector.

[1] M. Petyt, J. Lea, and G. H. Koopman, ''A finite element method for determining the acoustic modes of irregular shaped cavities,'' J. Sound Vib. **45**, 497–502 (1976).
[2] P. D. Joppa and I. M. Fyte, ''A finite element analysis of the impedance properties of irregular shaped cavities with absorptive boundaries,'' J. Sound Vib. **56**, 61–69 (1978).

3320   J. Acoust. Soc. Am., Vol. 101, No. 6, June 1997

J. Missaoui and L. Cheng: Integro-modal approach   3320

[3] T. L. Richards and S. K. Jha, ''A simplified finite element method for studying acoustic characteristics inside a car cavity,'' J. Sound Vib. **63**, 61–72 (1979).

[4] J. F. Unruh, ''A finite element subvolume technique for structural-borne interior noise prediction,'' J. Aircraft **17**, 434–441 (1980).

[5] E. H. Dowell, G. F. Gorman III, and D. A. Smith, ''Acoustoelasticity: General theory, acoustic natural modes and forced response to sinusoidal excitation, including comparison with experiment,'' J. Sound Vib. **52**, 519–542 (1977).

[6] C.-F. Chao, E. H. Dowell, and D. B. Bliss, ''Modal analysis of interior noise fields,'' in *Proceedings of the Vibrations Conference of the Design Engineering Technical Conferences* (ASME, New York, 1981), pp. 30–56.

[7] P. M. Morse and H. Feshbach, *Methods of Theoretical Physics*, Vol. II (McGraw-Hill, New York, 1953).

[8] G. P. Succi, ''The interior acoustic field of an automobile cabin,'' J. Acoust. Soc. Am. **81**, 1688–1694 (1987).

[9] C. R. Fuller, ''Structural influence of cabin floor on sound transmission into propeller aircraft-analytical investigation,'' AIAA Paper 86-1940 (1986).

[10] L. D. Pope, ''On the prediction of propeller tone sound levels and gradients in an airplane cabin,'' J. Acoust. Soc. Am. **88**, 2755–2765 (1990).

[11] J. Missaoui, L. Cheng, and M. J. Richard, ''Free and forced vibration of a cylindrical shell with a floor partition,'' J. Sound Vib. **190**, 21–40 (1996).

[12] L. D. Pope, E. G. Wilby, and J. F. Wilby, ''Propeller aircraft interior noise model,'' NASA CR 3813 (1984).

[13] L. D. Pope, E. G. Wilby, and J. F. Wilby, ''Analytical predictor of the interior noise for cylindrical models of aircraft fuselage for prescribed exterior noise fields. Phase II: Models for sidewall trim, stiffened structures, and cabin acoustics with floor partition,'' NASA CR 165869 (1982).